THE JOURNAL OF BIOLOGICAL CHEMISTRY VOL. 287, NO. 16, pp. 13407–13421, April 13, 2012

Direct Observation of Translocation in Individual DNA Polymerase Complexes*[S]

Received for publication, December 29, 2011, and in revised form, February 8, 2012 Published, JBC Papers in Press, February 29, 2012, DOI 10.1074/jbc.M111.338418

Joseph M. Dahl[‡], Ai H. Mai[‡], Gerald M. Cherf[‡], Nahid N. Jetha[§], Daniel R. Garalde[¶], Andre Marziali[§], Mark Akeson[‡], Hongyun Wang[‖1], and Kate R. Lieberman[‡2]

From the [‡]Department of Biomolecular Engineering, the [‖]Department of Applied Mathematics and Statistics, and the [¶]Department of Computer Engineering, Baskin School of Engineering, University of California, Santa Cruz, California 95064 and the [§]Department of Physics and Astronomy, University of British Columbia, Vancouver, British Columbia V6T 1Z1, Canada

Background: DNA polymerases translocate along DNA by one nucleotide in each catalytic cycle.
Results: The DNA polymerase translocation step is observed with single nucleotide and submillisecond precision.
Conclusion: DNA polymerase complexes fluctuate between pre- and post-translocation states and are rectified to the post-translocation state by dNTP.
Significance: These results provide insight into the translocation mechanism and its integration into the DNA polymerase catalytic pathway.

Complexes of phi29 DNA polymerase and DNA fluctuate on the millisecond time scale between two ionic current amplitude states when captured atop the α-hemolysin nanopore in an applied field. The lower amplitude state is stabilized by complementary dNTP and thus corresponds to complexes in the post-translocation state. We have demonstrated that in the upper amplitude state, the DNA is displaced by a distance of one nucleotide from the post-translocation state. We propose that the upper amplitude state corresponds to complexes in the pre-translocation state. Force exerted on the template strand biases the complexes toward the pre-translocation state. Based on the results of voltage and dNTP titrations, we concluded through mathematical modeling that complementary dNTP binds only to the post-translocation state, and we estimated the binding affinity. The equilibrium between the two states is influenced by active site-proximal DNA sequences. Consistent with the assignment of the upper amplitude state as the pre-translocation state, a DNA substrate that favors the pre-translocation state in complexes on the nanopore is a superior substrate in bulk phase for pyrophosphorolysis. There is also a correlation between DNA sequences that bias complexes toward the pre-translocation state and the rate of exonucleolysis in bulk phase, suggesting that during DNA synthesis the pathway for transfer of the primer strand from the polymerase to exonuclease active site initiates in the pre-translocation state.

DNA polymerases are molecular motors that catalyze template-dependent DNA replication. In each catalytic cycle, these enzymes translocate along their DNA substrate by the distance of a single nucleotide. Accurate translocation is essential to prevent frameshift mutations and thus fundamental to the fidelity of DNA replication. Fidelity also depends upon the specific incorporation of the deoxynucleoside triphosphate (dNTP) complementary to the templating base in the polymerase active site. DNA polymerases achieve fidelity through two mechanisms. First, in each catalytic cycle they select complementary dNTP via a series of conformational checkpoints that precedes the covalent step of phosphodiester bond formation (1–3). One of these conformational rearrangements is well characterized through comparison of the crystal structures of DNAP-DNA complexes formed in the absence or presence of complementary dNTP. The general architecture of the DNA polymerase domain is highly conserved and resembles a partially closed right hand, comprising three subdomains (4–7). The palm subdomain contains residues required for the chemistry of catalysis, whereas the thumb subdomain positions the primer-template duplex in the active site. The fingers subdomain contains residues essential for binding incoming nucleotide substrates. In crystal structures of complexes containing complementary dNTP, the position of the fingers subdomain differs from its position in the binary complex structures; elements of this subdomain move in toward the active site cleft to achieve a tight steric fit with the nascent base pair.

A second mechanism that contributes to the fidelity of replication occurs after an incorrect dNMP residue is incorporated into the primer strand. Progression to the next nucleotide addition cycle is slowed, allowing many DNA polymerases to recognize the mismatch and transfer the primer strand to a 3′-5′-exonuclease active site, where the incorrect dNMP is hydrolytically excised. The trimmed primer strand is then transferred back to the polymerase active site for synthesis to resume. The exonuclease active site is located in a separate domain (or in some cases, a separate subunit) of the enzyme; in A and B family polymerases the exonuclease site is separated from the polymerase active site by 30–40 Å

* This work was supported, in whole or in part, by National Institutes of Health Grants 1R01GM087484-01A2 from NIGMS (to K. R. L. and M. A.) and 1RC2HG005553 (to M. A.) and R01HG003248 (to N. N. J. and A. M.) from NHGRI. This work was also supported by National Science Foundation Grant DMS-0719361 (to H. W.).
[S] This article contains supplemental Figs. S1–S6 and supplemental experimental analysis procedure.
[1] To whom correspondence may be addressed: Dept. of Applied Mathematics and Statistics, Baskin School of Engineering, University of California, Santa Cruz, 1156 High St., MS SOE2, Santa Cruz, CA 95064. E-mail: hongwang@soe.ucsc.edu.
[2] To whom correspondence may be addressed: Dept. of Biomolecular Engineering, Baskin School of Engineering, University of California, Santa Cruz, 1156 High St., MS SOE2, Santa Cruz, CA 95064. Tel.: 831-459-5157; Fax: 831-459-4482; E-mail: krlieberman@gmail.com.

(4, 5, 8, 9–11). Primer strand transfer requires that several base pairs of the primer-template duplex be melted. Transfer from the polymerase to the exonuclease active site can occur via an intermolecular or intramolecular mechanism (12, 13), and one or more intermediates have been implicated in the transfer pathway (14–16).

Optimum balance between speed and accuracy in replication requires that the process of primer strand transfer between the polymerase and exonuclease active sites be tightly coordinated. A detailed description of the kinetic and structural mechanisms that govern the transfer pathway, and how this pathway is integrated into the nucleotide addition cycle, is required to understand how this balance is achieved. At what step in the nucleotide addition cycle is the transfer reaction initiated? How does it relate to other steps that occur following phosphodiester bond formation, including pyrophosphate release, fingers opening, and translocation?

The B-family DNA polymerase from bacteriophage phi29 contains 5′-3′-polymerase and 3′-5′-exonuclease functions within a single ~66.5-kDa protein chain (17, 18). This polymerase catalyzes the processive replication of tens of kilobases of DNA *in vitro* without the need for accessory proteins such as sliding clamps or helicases. Strand transfer between the polymerase and exonuclease active sites of phi29 DNAP[3] in bulk phase occurs via an intramolecular process (12). In optical trap experiments, it has been shown that a transition from processive synthesis to processive exonucleolysis by phi29 DNAP can be induced by high levels of tension on the template strand. Kinetic modeling led to the proposal of at least two intermediates in the switch from the polymerization to the exonucleolytic reactions (16).

Processive DNA synthesis catalyzed by phi29 DNAP can be monitored with single nucleotide resolution using the α-hemolysin (α-HL) nanopore (19). In the current study, we have directly observed a fluctuation across the translocation step on the millisecond time scale for individual phi29 DNAP-DNA complexes captured atop the nanopore. The data suggest a model in which polymerase translocation is driven by Brownian thermal motion. Binary complexes fluctuate between the pre-translocation and post-translocation states and can be rectified to the post-translocation state by the binding of complementary dNTP. Active site-proximal sequences in DNA substrates bearing fully base-paired duplexes affect the equilibrium between the two states. There is a correlation between the dwell time of phi29 DNAP-DNA complexes in the pre-translocation state on the nanopore and the relative efficiency of DNA substrates in bulk phase for both the exonuclease reaction and for pyrophosphorolysis, a catalytic reaction that occurs in the polymerase active site in the pre-translocation state. These data implicate the pre-translocation state as a branch point in the pathway for primer strand transfer from the polymerase to exonuclease active sites, suggesting that during DNA synthesis the commitment to transfer the primer strand to the exonuclease site is made prior to the translocation step. Thus, the probability of strand transfer may be determined in part by the probability of pre-translocation state occupancy following nucleotide addition.

[3] The abbreviations used are: DNAP, DNA polymerase; α-HL, α-hemolysin.

EXPERIMENTAL PROCEDURES

DNA and Enzymes—DNA oligonucleotides were synthesized at the Stanford Protein and Nucleic Acid Facility and were purified by denaturing PAGE. DNA hairpins were annealed prior to experiments by heating at 90 °C for 4 min followed by snap cooling in ice water. Results indistinguishable from those presented for experiments with the substrate in Fig. 1*B* were obtained using a two-piece primer-template hybrid bearing the same active site-proximal sequences and template abasic reporter. Wild type phi29 DNAP was obtained from Enzymatics (Beverly, MA). The N62D and D12A/D66A mutant phi29 DNAP enzymes were obtained from XPol Biotech (Madrid, Spain). Experiments with the mutant proteins were conducted at the University of British Columbia.

Nanopore Methods—Nanopore experiments were conducted as described (19, 20, 22, 23, 30) in buffer containing 10 mM K-Hepes, pH 8.0, 0.3 M KCl, and 1 mM EDTA. DTT and $MgCl_2$ were added to the *cis* chamber to final concentrations of 1 and 11 mM, respectively. Ionic current was measured using an integrating patch clamp amplifier (Axopatch 200B, Molecular Devices) in voltage clamp mode. Data were sampled using an analog-to-digital converter (Digidata 1440A, Molecular Devices) at 100 kHz in whole-cell configuration and filtered at 5 kHz using a low pass Bessel filter.

Data Analysis—Histograms of all sampled amplitude data points were generated with Clampfit software (Molecular Devices) at 0.2 pA bin width. Histograms in Fig. 2*B* were fit to a single term Gaussian function using the Levenberg-Marquardt search algorithm provided in Clampfit; histograms in the remaining figures (Fig. 1*D*, Fig. 4*B* and supplemental Figs. S2 and S4) were fit to a two-term Gaussian function using the same search algorithm. The probability of the lower amplitude state is calculated using the maximum likelihood estimation on the samples of measured amplitudes (supplemental data). Mathematical modeling and statistical analysis of the data are detailed in the supplemental data.

Bulk Phase Enzyme Assays—Exonuclease and pyrophosphorolysis assays shown in Figs. 4 and 5 were conducted as described under "Results" and in the legends to Figs. 4 and 5. Reactions were terminated at the indicated times with buffer-saturated phenol. Following extraction and ethanol precipitation, reaction products were dissolved in 7 M urea, 0.1× Tris borate-EDTA (TBE) and resolved in gels containing 22% acrylamide:bisacrylamide (19:1), 7 M urea, and 1× TBE. Gels were visualized on a UVP gel documentation system. Band intensities were quantified using NIH ImageJ software.

RESULTS

The α-HL nanopore has emerged as a tool for distinguishing among DNAP-DNA complexes in different functional states at the single molecule level with high spatial and temporal resolution (19, 20–23). In the nanopore device, a single α-HL nanopore is inserted in a lipid bilayer that separates two chambers (termed *cis* and *trans*) containing buffer solution (Fig. 1*A*). Ionic current through the nanopore is carried by K^+ and Cl^- ions, and a patch clamp amplifier applies voltage and measures ionic current. A typical current trace for a captured binary com-

plex between wild type phi29 DNAP and a DNA substrate (Fig. 1*B*, *DNA1*), formed in buffer containing 10 mM $MgCl_2$ and captured at 180 mV applied potential, is shown in Fig. 1*C*. Schematics above the current trace illustrate the sequence of events. A decrease in ionic current through the nanopore from the open channel level (Fig. 1*C*, *i*) occurs when the phi29 DNAP-DNA complex is captured (Fig. 1*C*, *ii*). The enzyme is too large to enter the nanopore vestibule and thus holds the duplex portion of the DNA substrate atop the pore. In this state, the DNA template strand is suspended through the pore lumen, which is wide enough to accommodate single-stranded but not duplex DNA.

Phi29 DNAP-DNA complexes reside atop the nanopore for several seconds at 180 mV applied potential (Fig. 1*C*, *ii*). During this period, binary complexes formed with the DNA1 substrate fluctuate between an upper amplitude level centered at ~32 pA and a lower amplitude level centered at ~26 pA (Fig. 1, *C*, *ii*, and *D*, *top panel*). These amplitude fluctuations continue until the onset of complex dissociation, which occurs via voltage-promoted duplex unzipping in the absence of Mg^{2+} or via exonucleolytic digestion when Mg^{2+} is present (Fig. 1*C*, *iii*–*v*, and Ref. 19). Following enzyme dissociation and electrophoresis of the remaining DNA through the pore, the open channel current is restored (Fig. 1*C*, *vi*) and another complex can be captured.

When dGTP (complementary to the dCMP residue at $n = 0$ of the template strand) was titrated into the nanopore chamber, it caused a concentration-dependent increase in the fraction of time that phi29 DNAP-DNA complexes spent in the lower of the two amplitude states observed for the binary complex (Fig. 1*D*, *insets*, *current traces*). The equilibrium between the two states was determined by generating histograms of all sampled amplitude data points (Fig. 1*D*, *blue curves*) and fitting them to a function of two Gaussian modes to calculate the area under each Gaussian mode (Fig. 1*D*, *red curves*). The equilibrium between the two amplitude states is expressed as

p = probability of the lower amplitude state.

Throughout this study, p is reported in the format of means ± S.E. For example, the average fraction under the lower amplitude peak, determined from histograms of 27 individual phi29 DNAP-DNA binary complexes captured at 180 mV (such as those shown in Fig. 1*C* and in the *top panel* (0 μM dGTP) in Fig. 1*D*), was $p = 0.14 \pm 0.002$. The equilibrium between the two amplitude states was not affected by the presence of non-complementary dNTPs (supplemental Fig. S1). Stabilization of the lower amplitude state specifically required dNTP complementary to the templating base in the polymerase active site. Thus the lower of the two amplitude states can be assigned as one in which the primer-template junction is in the polymerase active site in the post-translocation state.[4]

Physical Nature of Fluctuations between the Two Amplitude States—The ionic current transitions that occur when phi29 DNAP-DNA complexes are held atop the nanopore in an applied field could have two different causes, which are not mutually exclusive. They could be due to conformational changes in the phi29 DNAP-DNA complex atop the pore that alter the extent to which the complex impedes ion flow into the channel. Alternatively, the amplitude oscillations could be caused by a movement of the DNA relative to the nanopore that alters the position of the template strand in the pore lumen. The five consecutive abasic (1′,2′-H) residues in the template strand of the DNA1 substrate (Fig. 1*B*) serve as a reporter that modulates the ionic current blockade of DNAP-DNA complexes. They allow more current to flow through the channel than a strand composed of normal DNA residues alone. The extent to which the abasic reporter augments the amplitude of captured complexes depends upon its position relative to the limiting aperture of the nanopore lumen. Thus, the abasic residues can report on the position of DNA in captured complexes and on the direction and distance of movement of the DNA template with respect to the enzyme and nanopore during synthetic and degradative reactions (19, 22, 23).

To determine the contribution of template displacement to the amplitude oscillations, we formed phi29 DNAP complexes with a substrate that lacked the abasic reporter group and that contained poly(dCMP) spanning template positions +5 to +29 (the entire length of the segment suspended through the nanopore; see Fig. 2*A*). In this substrate, the DNA sequences that interact with the enzyme in the duplex region and in the template strand from positions $n = 0$ to +4 were identical to those in the DNA1 substrate (Fig. 1*B*). No amplitude transitions were discernable when complexes formed with the DNA substrate lacking the abasic reporter group (see *current traces* in Fig. 2*B*, *insets*) were captured. Histograms of all sampled amplitude points fit well to a single Gaussian distribution (Fig. 2*B*) for the binary complexes formed with this substrate and when dGTP was titrated into the chamber. The same results where obtained with substrates in which poly(dAMP) or poly abasic residues spanned +5 to +29 of the template strand (supplemental Fig. S2, *A* and *B*). Thus, the ability to detect the state fluctuations of complexes atop the pore is dependent on the presence of a reporter group in the DNA template strand that is suspended through the nanopore lumen. The direct contribution to the transitions in the measured signal caused by changes in the extent to which the complex atop the pore directly impedes the entry of ions into the channel is negligible. The oscillations in ionic current amplitude detected for phi29 DNAP complexes are caused by the displacement of the template strand in the lumen, reported by the appropriately placed abasic residues.

Mapping experiments have established that when phi29 DNAP complexes formed with DNA1 (Fig. 1*B*) are captured, the abasic residues that span positions +8 through +12 of the template are positioned just above the limiting aperture of the pore lumen (19). With this DNA substrate, if the template strand moves closer to the complex atop the pore, the ionic

[4] Throughout this work, we have used the terms pre-translocation state and post-translocation state to refer to the position of the polymerase with respect to the covalent state of the DNA substrate for complexes in which the primer-template junction is in the polymerase active site. Thus, the post-translocation state refers to either binary (polymerase-DNA) or ternary (polymerase-DNA-dNTP) complexes in which the 3′-terminus of the base-paired primer strand occupies the priming site, with the templating base at position $n = 0$ available for base-pairing with incoming dNTP. Accordingly, the pre-translocation state refers to complexes in which the 3′-terminus of the base-paired primer strand occupies the nucleotide insertion site.

current decreases as the abasic block is moved further from the limiting aperture. Conversely, movement of the template strand away from the enzyme complex atop the pore result in an ionic current amplitude increase as the abasic block is moved closer to the limiting aperture. Therefore, when complexes formed with the DNA1 substrate transition from the lower amplitude, post-translocation state (Fig. 2*C*, *i*) to the higher amplitude state (Fig. 2*C*, ii), the template strand moves away from the complex atop the pore (further toward the *trans* chamber). This assignment of the direction of the template

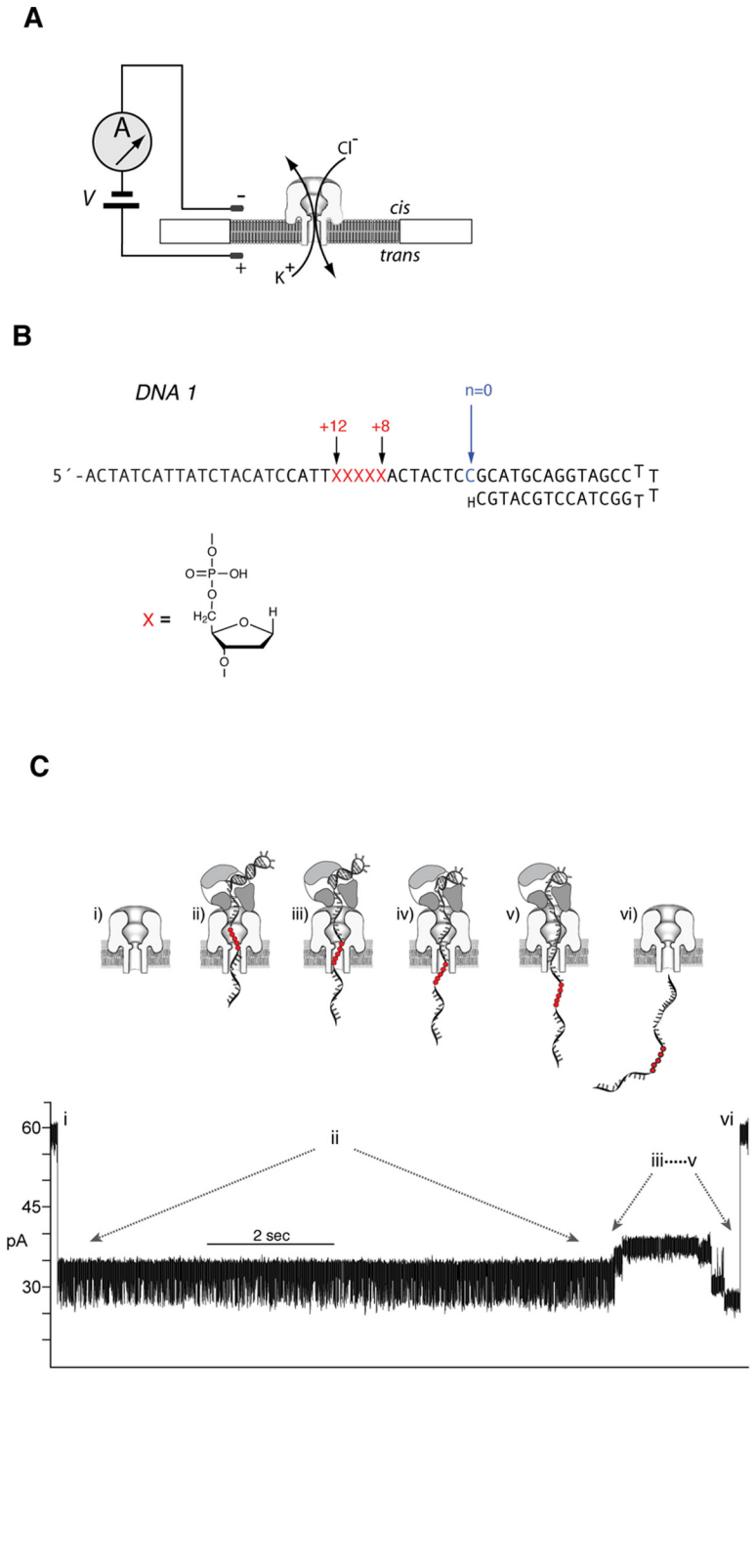

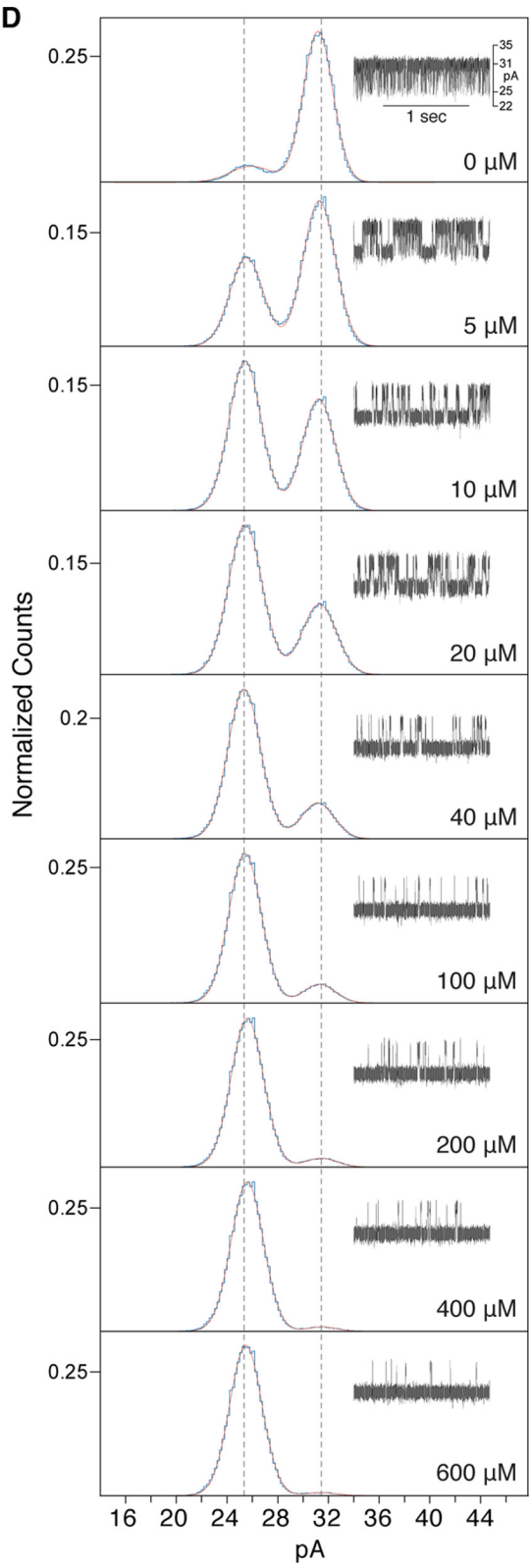

movement was corroborated by the results of experiments in which phi29 DNAP complexes were formed with a DNA substrate bearing an abasic reporter spanning template positions +13 to +17 (supplemental Fig. S2, *C* and *D*).

Distance of the Template Movement—To evaluate the distance of the template displacement that occurs when phi29 DNAP complexes reside atop the nanopore and transition between the two amplitude states, we used three DNA substrates in which an abasic reporter was embedded at different positions in a template strand that otherwise consisted of poly C from positions +5 to +34. In the three DNA substrates, the abasic block spanned positions +7 to +11 (Fig. 2*D*, *i*), +8 to +12 (Fig. 2*D*, *ii*), or +9 to +13 (Fig. 2*D*, *iii*) of the template. The poly C flanking the abasic blocks minimizes the effects of the DNA sequence on ionic current amplitude. DNA sequences in the duplex region of these substrates and in the template strand from positions $n = 0$ to +4 were identical to those in the DNA1 substrate (Fig. 1*B*). Complexes formed with each of these three DNA substrates exhibited amplitude oscillations (supplemental Fig. S3) similar to those observed for the DNA1 substrate. When phi29 DNAP-DNA complexes formed with substrates bearing these three abasic configurations are captured, the abasic block is positioned above the limiting aperture of the pore lumen (19). As observed with the DNA1 substrate, with each of the three substrates the lower amplitude state was stabilized by the addition of dGTP (supplemental Fig. S3), indicating that the direction that the template moves in the transition from one functional state to the other is the same among all of the complexes.

In the presence of dGTP, the lower of the two amplitude states can be considered a reference point in which complexes formed with the substrates in Fig. 2*D*, *i–iii*, are in equivalent functional states (with the primer-template junction bound in the polymerase active site in the post-translocation state). Thus, when complexes formed with the substrate bearing the abasic block from positions +9 to +13 are in the lower amplitude state, the position of the abasic block in the pore lumen is displaced by a single nucleotide relative to the lower amplitude state of complexes formed with the substrate in which the abasic block spans positions +8 to +12. The same is true when complexes formed with the substrate bearing the abasic block from positions +8 to +12 are compared with complexes formed with the substrate bearing the abasic block from positions +7 to +11.

We compared complexes in which the abasic block in the template was displaced by the distance of a single nucleotide, in experiments in which two DNA substrates (with the abasic block spanning either +7 to +11 and +8 to +12 *or* +8 to +12 and +9 to +13) were present in the *cis* chamber at the same time, minimizing the small effects of experiment-to-experiment variation on the comparisons. A plot of the upper and lower amplitude peaks from histograms of all the sampled amplitude points for numerous complexes shows that the upper amplitude state for complexes formed with the substrate bearing the abasic block from positions +7 to +11 corresponds closely to the lower amplitude state of complexes formed with the substrate in which the abasic block spans positions +8 to +12 (Fig. 2*E*). Analogously, the upper amplitude state for complexes formed with the substrate bearing the abasic block from positions +8 to +12 corresponds closely to the lower amplitude state of complexes formed with the substrate with the abasic block from positions +9 to +13. These correspondences also hold when complexes are captured at higher voltages (Table 1). Fig. 2*F* shows a representative current trace from such an experiment, in which phi29 DNAP, 200 μM dGTP, and the substrates in Fig. 2*D*, *ii* and *iii*, were added to the pore chamber. Complexes were captured at 180 mV. The latter portion of the trace for a complex with the abasic reporter spanning +8 to +12 of the template is shown followed directly by the beginning portion of trace for the capture of a complex with the template abasic residues spanning +9 to +13 (Fig. 2*D*). The *dashed blue line* shows the close alignment of the upper amplitude state of the first complex with the lower amplitude of the second (Fig. 2*F*). Thus, when phi29 DNAP-DNA complexes move from the lower amplitude state (in which the primer-template junction is in the polymerase active site in the post-translocation state) to the upper amplitude state, the DNA moves with respect to the nanopore such that the template strand is displaced further away from the complex atop the pore by a distance of ~1 nucleotide (Fig. 2*C*).

Effects of Voltage and dNTP on phi29 DNAP-DNA Complexes—The equilibrium between the two amplitude states for captured phi29 DNAP-DNA complexes is dependent upon complementary dNTP in a concentration-dependent manner (Fig. 1*D*). The equilibrium between the states is also dependent upon the applied voltage, which exerts force on the DNA template strand. We used a four-state model to study the equilibrium properties of the amplitude transitions

FIGURE 1. **Complexes of phi29 DNAP captured in the α-HL nanopore.** In the nanopore device (*A*), a single α-HL nanopore is inserted in a ~25-μm-diameter lipid bilayer that separates two chambers (*cis* and *trans*) containing buffer solution. Current through the nanopore is carried by K^+ and Cl^- ions. A patch clamp amplifier applies voltage and measures ionic current. *B*, hairpin DNA substrate (DNA1) featuring a 14-base pair duplex region and a single-stranded template region of 35 nucleotides. The primer strand terminates with a 3′-ddCMP residue, and the template strand contains five consecutive abasic (1′,2′-H) residues spanning positions +8 to +12 (indicated as *red Xs* in the sequence). The structure of an abasic residue is shown below the DNA sequence. *C*, Representative current trace for a binary complex formed between phi29 DNAP and the DNA1 substrate captured at 180 mV applied potential in buffer containing 10 mM K-Hepes, pH 8.0, 0.3 M KCl, 1 mM EDTA, 1 mM DTT, and 11 mM $MgCl_2$. DNA and phi29 DNAP were added to the nanopore *cis* chamber to final concentrations of 1 and 0.75 μM, respectively. Schematics are labeled with *lowercase roman numerals* corresponding to those above the features in the current trace that they illustrate, which are described under "Results." In the schematics, the abasic residues are shown as *red circles*. *D*, amplitude histograms (*blue curves*) fit to a two-term Gaussian function (*red curves*) for phi29 DNAP-DNA complexes formed with the DNA1 substrate shown in *B* and captured at 180 mV applied potential. Current trace segments from within the measured events are shown as *insets* in the *upper right* of each histogram panel, and the concentration of dGTP in the nanopore chamber is indicated in the *lower right* of each panel. The average fraction (*p*) in the lower amplitude state for complexes captured under each condition in the experiment shown (given as means ± S.E. followed by number of complexes) was: 0 μM dGTP, $p = 0.14 \pm 0.002$, 27; 5 μM dGTP, $p = 0.38 \pm 0.011$, 10; 10 μM dGTP, $p = 0.52 \pm 0.01$, 16; 20 μM dGTP, $p = 0.69 \pm 0.013$, 17; 40 μM dGTP, $p = 0.8 \pm 0.007$, 11; 100 μM dGTP, $p = 0.89 \pm 0.004$, 9; 200 μM dGTP, $p = 0.94 \pm 0.002$, 10; 400 μM dGTP, $p = 0.97 \pm 0.002$, 8; 600 μM dGTP, $p = 0.98 \pm 0.001$, 9.

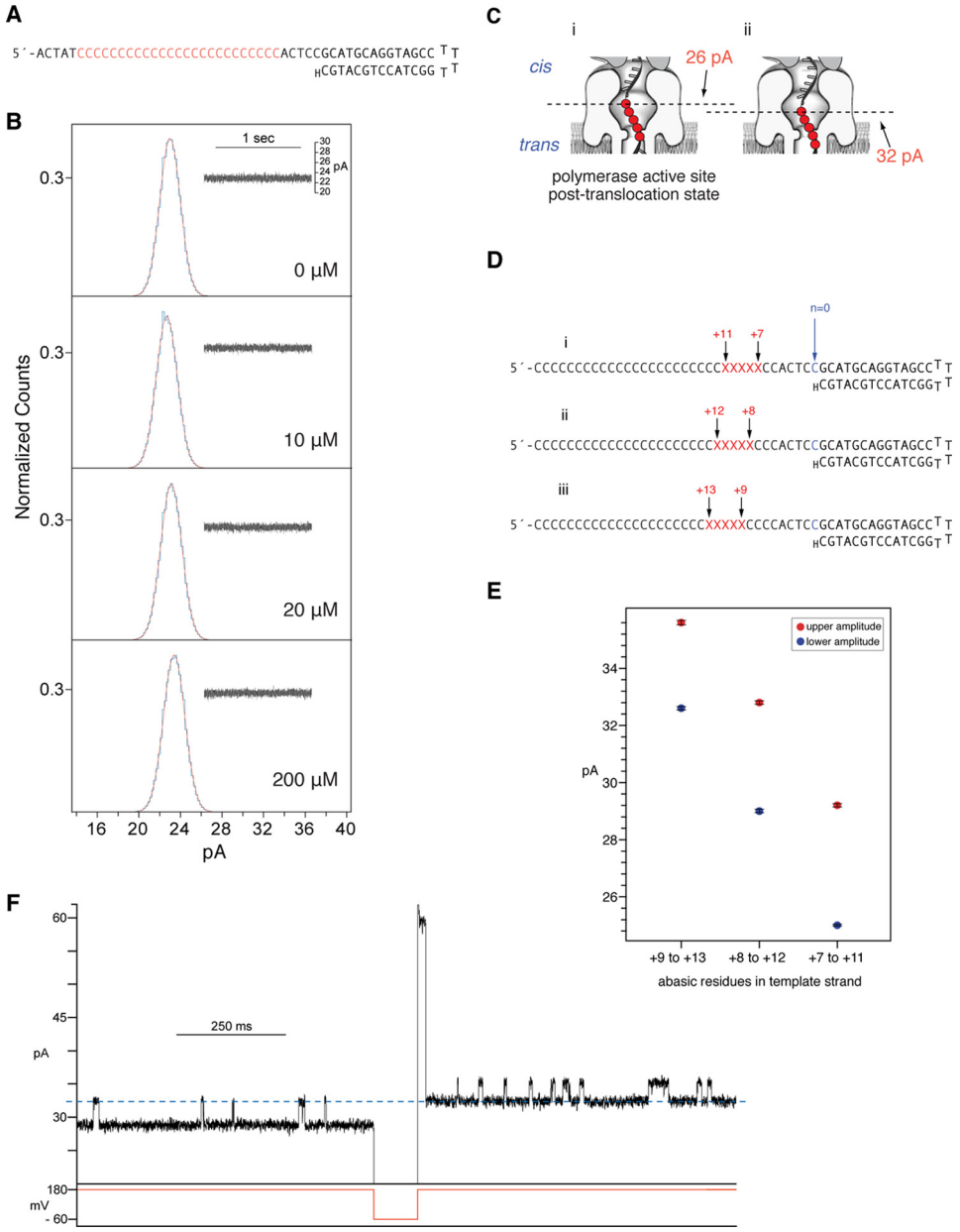

FIGURE 2. **The physical nature and distance of the fluctuations between the two amplitude states.** *A*, DNA substrate used to determine the physical cause of phi29 DNAP-DNA complex amplitude oscillations. The template strand of this substrate features poly(dCMP) from +5 to +29. The substrate is otherwise identical to DNA1 (shown in Fig. 1*B*). *B*, amplitude histograms (*blue curves*) shown with the fit to a single Gaussian function (*red curves*) for representative phi29 DNAP-DNA complexes formed with the substrate shown in *A* and captured at 180 mV applied potential. Current trace segments from within the measured events are shown as *insets* in the *upper right* of each histogram panel, and the concentration of dGTP in the nanopore chamber is indicated in the *lower right* of each panel. *C*, schematic illustration of the template displacement that occurs when phi29 DNAP complexes formed with the DNA1 substrate in Fig. 1*B* move from the lower amplitude state (*i*) (~26 pA at 180 mV applied potential) that can be stabilized by complementary dNTP to the upper amplitude state (*ii*) (~32 pA at 180 mV applied potential). In the transition from state *i* to *ii*, the template strand moves further away from the complex atop the pore (toward the *trans* chamber). This results in an amplitude increase as the abasic reporter is drawn closer to the limiting aperture of the nanopore lumen. *D*, DNA substrates used to determine the distance of the DNA template movement in the nanopore lumen during phi29 DNAP-DNA complex amplitude oscillations. The substrates feature abasic residues (indicated as *red Xs*) spanning template positions +7 to +11 (*i*), +8 to +12 (*ii*), or +9 to +13 (*iii*) embedded in a template strand that consists otherwise of poly(dCMP) from position +5 to +34. The DNA substrate sequences, including the entire duplex region and the template strand from positions $n = 0$ to +4, are otherwise the same as in DNA1 (Fig. 1*B*). *E*, plot of the average upper (*red circles*) and lower (*blue circles*) amplitudes for complexes formed with the substrates shown in *D*, captured at 180 mV. Values plotted are the average of the peak amplitudes from histograms of all sampled data points (measured from 10 to 15 s of current trace from each event) fit to a two-term Gaussian function. *Error bars* indicate the standard error of the mean. *F*, real-time current trace at 180 mV applied potential, showing the latter part of a capture event for a phi29 DNAP-DNA complex formed with the substrate shown in *Dii* followed directly by a capture of a complex with the substrate shown in *Diii*. Both DNA substrates (0.5 μM each), phi29 DNAP (1 μM), and 200 μM dGTP were present in the *cis* chamber. To maximize the number of complexes sampled during individual experiments, events that lasted longer than 30 s were terminated by a voltage reversal to −60 mV to eject the complex from atop the pore. Amplitude assignments for experiments in which two DNA substrates were present were verified in experiments in which DNA substrates were examined individually.

(Fig. 3*A*). As detailed in the supplemental data, along the direction of DNA displacement (amplitude change), we labeled the upper amplitude state as state 1 and the lower amplitude state as state 2. Along the direction of dGTP binding/dissociation, the DNAP-DNA complex has two states: a binary complex (denoted by *B*) and a ternary complex

TABLE 1

Template strand movement between the two amplitude states in phi29 DNAP-DNA complexes

In each row, the values reported for complexes with the two DNA substrates were obtained from experiments in which phi29 DNAP (either the wild type or the N62D mutant, as indicated) and both DNA substrates, along with dGTP at the indicated concentration, were present in the nanopore chamber. Complexes were captured at the indicated applied potential. Rows that have the same dGTP concentration and applied potential are from independent experiments.

phi29 DNAP	[dGTP]	mV	Upper amplitude state with +8 to +12 abasic reporter[a]	Lower amplitude state with +9 to +13 abasic reporter[b]
	μM		*pA* ± *S.E.*	*pA* ± *S.E.*
Wild type	40	180	31.9 ± 0.03	31.7 ± 0.05
	40	180	32.6 ± 0.07	32.5 ± 0.06
	40	180	32.6 ± 0.02	32.4 ± 0.07
	40	190	36 ± 0.04	35.9 ± 0.09
	40	200	39.1 ± 0.05	39.2 ± 0.07
	40	210	42.7 ± 0.02	42.8 ± 0.04
	40	220	46 ± 0.05	46.1 ± 0.09
	200	180	32.1 ± 0.03	31.9 ± 0.07
	200	180	32.8 ± 0.03	32.6 ± 0.07
	200	180	32.9 ± 0.1	32.6 ± 0.08
	200	190	35.5 ± 0.08	35.4 ± 0.04
	200	190	36.3 ± 0.06	36.1 ± 0.04
	200	200	38.3 ± 0.04	38.2 ± 0.03
	200	210	42 ± 0.04	41.9 ± 0.07
	200	220	45.2 ± 0.06	45.4 ± 0.06
	200	230	49.1 ± 0.11	49.1 ± 0.1
N62D	40	180	33.5 ± 0.03	33.2 ± 0.09
	40	190	36.6 ± 0.03	36.5 ± 0.06
	40	200	39.9 ± 0.02	39.9 ± 0.03
	40	210	43.3 ± 0.03	43.3 ± 0.03
	40	220	47.1 ± 0.04	47.2 ± 0.04
	200	180	33.1 ± 0.05	32.8 ± 0.03
	200	190	36.3 ± 0.06	36 ± 0.03
	200	200	39.4 ± 0.06	39.2 ± 0.06
	200	210	42.6 ± 0.06	42.3 ± 0.06
	200	220	45.9 ± 0.08	45.6 ± 0.12

[a] Average amplitude of the upper amplitude peak determined from amplitude histograms fit to a two-Gaussian function for complexes formed between phi29 DNAP and the DNA substrate in Fig. 2*D*, *ii*.

[b] Average amplitude of the lower amplitude peak determined from amplitude histograms fit to a two-Gaussian function for complexes formed between phi29 DNAP and the DNA substrate in Fig. 2*D*, *iii*.

(denoted by *T*). Taking together the DNA displacement and dGTP binding, we have four possible states: B1, DNAP-DNA binary complex in the upper amplitude state; T1, DNAP-DNA ternary complex in the upper amplitude state; B2, DNAP-DNA binary complex in the lower amplitude state; and T2, DNAP-DNA ternary complex in the lower amplitude state.

Recall that p = equilibrium probability of the lower amplitude state ($B2 + T2$). In the supplemental information, we derived that

$$\log\left(\frac{p}{1-p}\right) = \log\left(\frac{1+\frac{[\mathrm{dGTP}]}{K_d^{(2)}}}{1+\frac{[\mathrm{dGTP}]}{K_d^{(1)}}}\right) - \frac{\Delta G_B}{k_B T} - \frac{\alpha}{k_B T}\cdot V \qquad \text{(Eq. 1)}$$

where $K_d^{(1)}$ is the dGTP binding affinity of state 1 (upper amplitude state); $K_d^{(2)}$ is the dGTP binding affinity of state 2 (lower amplitude state); ΔG_B is the free energy difference between states 1 and 2 at voltage = 0 and [dGTP] = 0; and $\alpha \cdot V$ is the effect of the voltage in changing the free energy difference.

The quantity $\log(p/(1-p))$, predicted to be a linear function of voltage in the model, is plotted in Fig. 3*B* for data collected at various dGTP concentrations. The fitting lines for different dGTP concentrations are parallel to each other and differ only by a shift in the vertical direction (Fig. 3*B*). This indicates that the distance of the DNA displacement associated with the transitions between the two amplitude states is not affected by dGTP binding; rather, dGTP binding simply changes the equilibrium between the two states. Importantly, the binding of dGTP does not result in a third state along the direction of displacement, validating our assignment of the lower amplitude state in the binary complex as the post-translocation state.

To study the dGTP binding affinities of complexes in the two amplitude states, we consider the normalized $p/(1-p)$, defined as $p/(1-p)$ divided by its value at [dGTP] = 0, for dGTP titrations conducted at various voltages (see supplemental material for details). The model predicts that the normalized $p/(1-p) = (1+[\mathrm{dGTP}]/K_d^{(2)})/(1+[\mathrm{dGTP}]/K_d^{(1)})$.

In particular, it predicts that the normalized $p/(1-p)$ is independent of the voltage. The data in Fig. 3*C* show that the normalized $p/(1-p)$ is indeed independent of the voltage, which validates the assumption that K_d of dGTP for each amplitude state is independent of the voltage. In Fig. 3*C*, the normalized $p/(1-p)$ is a linear function of [dGTP] up to at least 1200 μM (the highest dGTP concentration tested). This implies that $K_d^{(1)}$, the binding affinity of dGTP for the upper amplitude state, is greater than 1200 μM. The slope of the linear function gives the value of $K_d^{(2)}$, the binding affinity of dGTP for the lower amplitude, post-translocation state. A least square fitting yields $K_d^{(2)} \approx 1.4$ μM.

The very large value of $K_d^{(1)}$ is consistent with the proposal that dGTP does not bind to phi29 DNAP-DNA complexes in the upper amplitude state but instead binds to complexes only in the post-translocation state. Close inspection of current

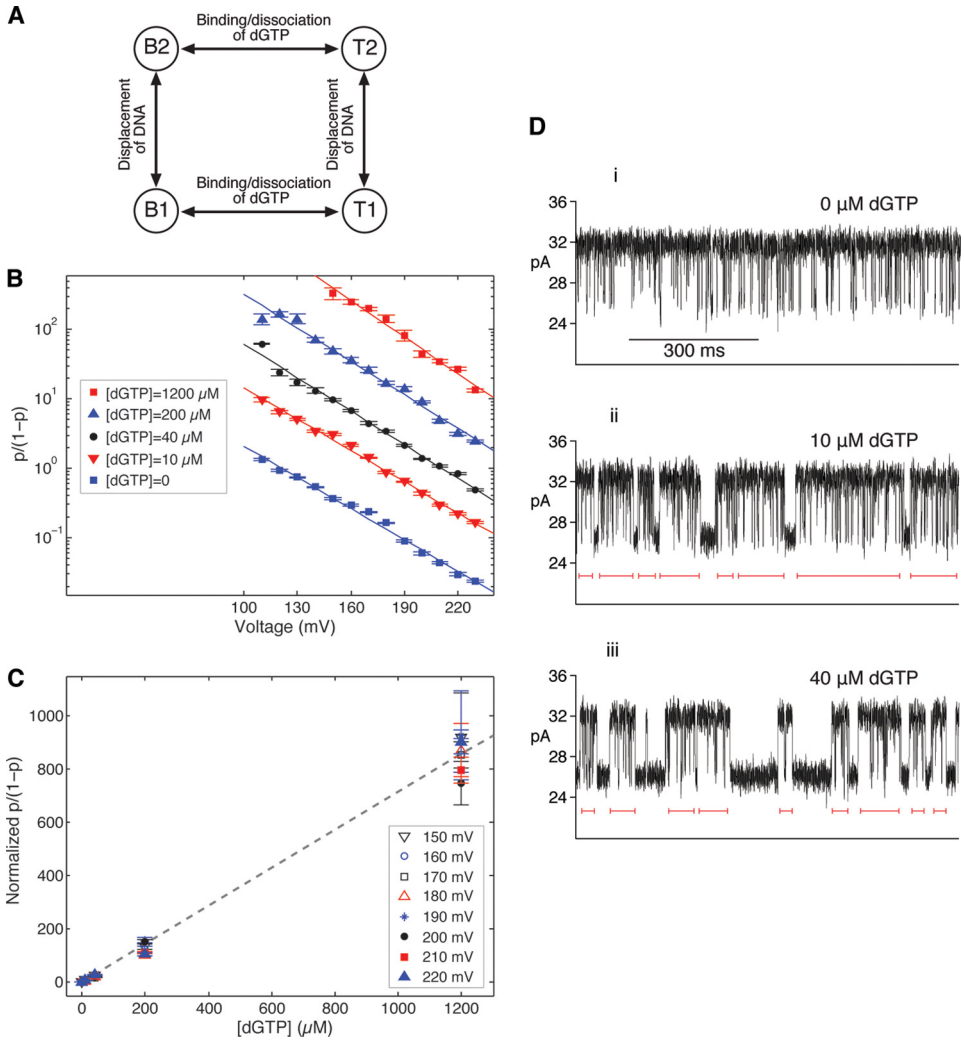

FIGURE 3. **Effects of voltage and dNTP on phi29 DNAP-DNA complex amplitude fluctuations.** *A*, four-state model for studying the equilibrium properties of amplitude transitions in phi29 DNAP-DNA complexes. State *B1* is the phi29 DNAP-DNA binary complex in the upper amplitude state; state *T1* is the phi29 DNAP-DNA-dGTP ternary complex in the upper amplitude state; state *B2* is the binary complex in the lower amplitude, post-translocation state; and state *T2* is the ternary complex in the lower amplitude, post-translocation state. *B*, the effect of voltage on $p/(1-p)$ for various complementary dNTP (dGTP) concentrations, where p is the probability of phi29 DNAP-DNA complexes formed with DNA1 occupying the lower amplitude, post-translocation state. *C*, the effect of dGTP on the normalized $p/(1-p)$ at various voltages. The normalized $p/(1-p)$ p) is defined under "Results." *D*, current traces for phi29 DNAP-DNA complexes formed with DNA 1 and captured at 180 mV in the presence of 0 (*i*), 10 (*ii*), or 40 μM (*iii*) dGTP. *Red lines* under segments of the traces in *ii* and *iii* indicate periods during which the complexes oscillate between the two amplitude states at rates that appear indistinguishable from the rates of the transitions in the binary complex (*i*).

traces at relatively low dGTP concentrations reveals periods (Fig. 3*D*, *ii* and *iii*, roughly indicated by *red lines*) during which complexes transition between the states with rates that cannot be distinguished from the binary complex transitions (Fig. 3*D*, *i*). These periods are punctuated by transitions in which the lower amplitude state is stabilized due to dGTP binding (Fig. 3*D*, *ii* and *iii*). Although these data do not formally rule out an effect of dGTP on the dwell time of complexes in the upper amplitude state, they suggest that dGTP affects the equilibrium solely by stabilizing the lower amplitude, post-translocation state.

Relationship between Upper Amplitude State and 3′-5′-Exonuclease Activity—We have shown that individual DNA substrate molecules with fully paired duplexes bearing 3′-H termini can be activated as substrates for primer extension in the presence of dNTPs, whereas phi29 DNAP-DNA complexes were held on the pore (19). This activation requires that the 3′-H ddNMP residue be excised in the exonuclease active site, and the trimmed primer strand, with its newly formed 3′-OH terminus, be transferred to the polymerase active site for synthesis to ensue. The characteristic amplitude fluctuations at the start of the capture events for these complexes (prior to ddNMP excision), to and from a state that can be stabilized by incoming dNTP, indicates that they initially reside at least part of the time in the polymerase active site. Thus, for synthesis to ensue, primer strand transfer in both directions between the polymerase and exonuclease active sites must occur at least once while these complexes reside atop the pore.

To address whether there was a relationship between the amplitude fluctuations of phi29 DNAP-DNA complexes atop the nanopore and exonucleolytic activity, we exploited the effect of DNA sequences on the amplitude fluctuations. The equilibrium of phi29 DNAP-DNA complexes between the upper and lower amplitude states can be modulated by DNA

sequences in both the duplex and single-stranded portions of the DNA substrate that are proximal to the polymerase active site (Fig. 4). We will present a detailed analysis of the effects of active site-proximal sequences on amplitude state equilibria elsewhere; here we have exploited the differences that are exhibited in complexes formed with three DNA substrates. In the first substrate (DNA1), the −2 primer-template base pair is G-C and the $n = 0$ residue is dCMP (Fig. 4*A*); this is the substrate featured in Fig. 1, *C* and *D*, for which the equilibrium fraction in the lower amplitude state for binary complexes captured at 180 mV is $p = 0.14 \pm 0.002$. For the second DNA substrate (Fig. 4*A*, *DNA2*), the −2 base pair is T-A and the $n =$

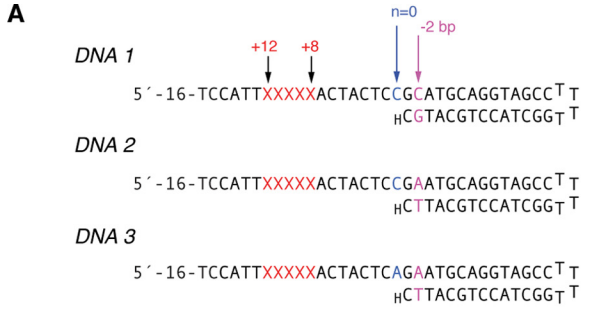

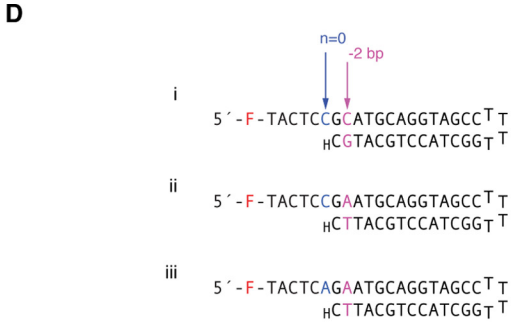

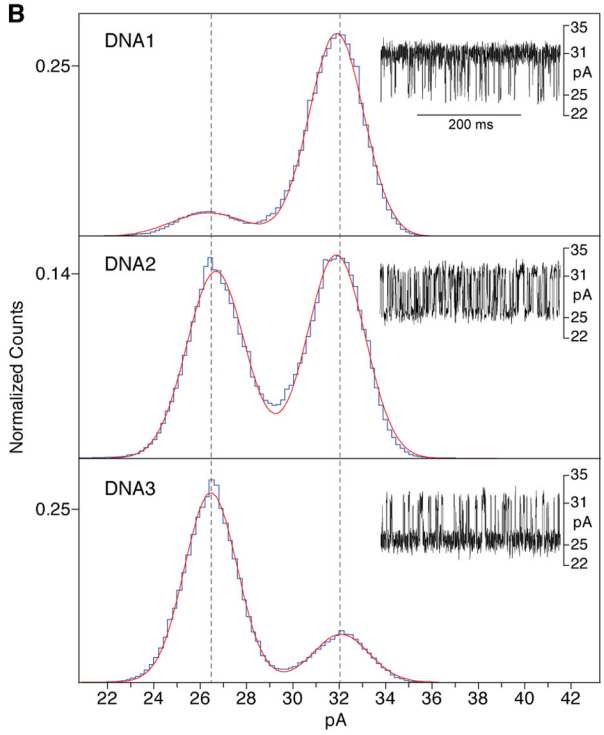

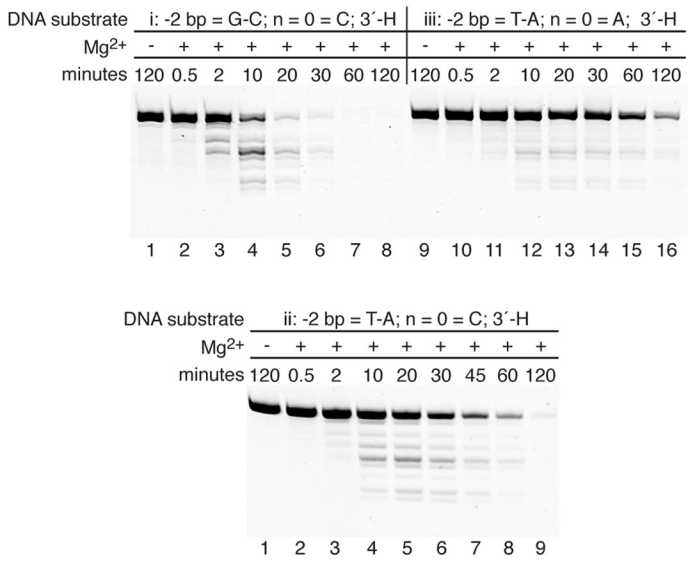

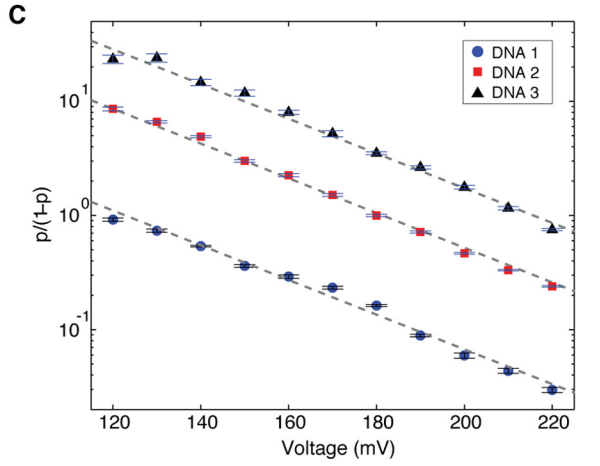

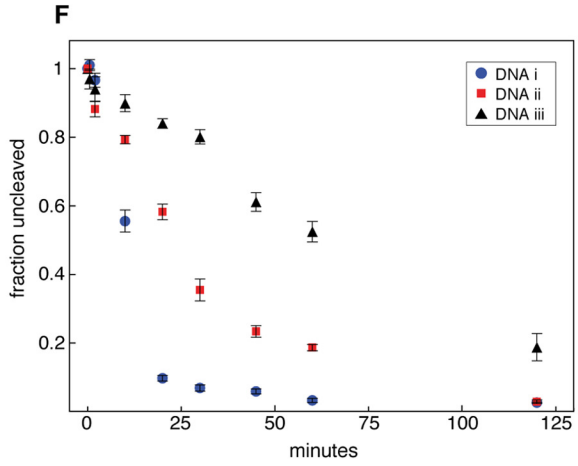

0 residue is dCMP. When binary complexes formed with this substrate are captured at 180 mV, the equilibrium fraction in the lower amplitude state is $p = 0.5 \pm 0.024$. In the third DNA substrate (Fig. 4*A*, *DNA3*), the −2 base pair is T-A and the $n = 0$ residue is dAMP. For binary complexes formed with this substrate and captured at 180 mV, the equilibrium fraction in the lower amplitude state is $p = 0.77 \pm 0.005$.

Representative histograms and current traces for binary complexes formed between wild type phi29 DNAP and each of the three substrates, captured at 180 mV, are compared in Fig. 4*B*. The dNTP complementary to $n = 0$ for DNA2 (dGTP) caused a concentration-dependent increase in the fraction of time that complexes spent in the lower amplitude state (not shown); dTTP, complementary to $n = 0$ for DNA3, caused a concentration-dependent increase in the fraction of time that phi29 DNAP-DNA3 complexes occupied the lower amplitude state (supplemental Fig. S4). This confirms that the lower amplitude state corresponds to the post-translocation state for complexes formed with each of the three DNA substrates. When the quantity $p/(1 - p)$ is plotted as a function of voltage for binary complexes formed with each of the three DNA substrates, the fitting lines are parallel to each other, differing only by a shift in the vertical direction (Fig. 4*C*). This indicates that the equilibrium between the two amplitude states, but not the distance of the DNA displacement associated with the transitions between the states, is affected by the active site-proximal sequences.

We compared DNA substrates bearing the three different sequences in exonuclease assays using 5′-fluorescein-labeled DNA hairpins bearing the same active site-proximal sequences as those used in the nanopore assays (Fig. 4*D*). There was a correlation between the extent to which active site-proximal sequences biased complexes toward the upper amplitude state and the propensity for the first exonucleolytic cleavage to occur in the bulk phase (Fig. 4, *E* and *F*). For example, after 10 min at 21 °C, 55.5 ± 3.2% of the substrate shown in Fig. 4*D*, *i*, remained intact; 79.3 ± 1.2% of the substrate shown in Fig. 4*D*, *ii*, remained intact; and 89.9 ± 2.5% of the substrate in Fig. 4*D*, *iii*, was uncleaved. After 60 min, these fractions were 3.2 ± 0.6%, 18.6 ± 0.9%, and 52.4 ± 3% for the substrates in Fig. 4*D*, *i*, *ii*, and *iii*, respectively (determined from four independent experiments and given with standard errors). This DNA sequence-dependent effect on the rate of the first exonucleolytic cleavage was also observed in buffer containing 150 mM KCl (supplemental Fig. S4). Identical results were obtained whether or not substrates were preincubated with phi29 DNAP prior to initiation of the reactions by the addition of Mg2+, indicating that the difference in activity among the three substrates was not due to a difference in the rate of phi29 DNAP binding to the different substrates.

The experiments shown in Fig. 4 suggest a correlation between the amplitude fluctuations observed on the nanopore for complexes held under force and bulk phase enzyme function absent force. The data suggest that the upper amplitude state is either one in which the primer strand has been transferred to the exonuclease active site (but is not cleaved and returns repeatedly to the polymerase active site), or it is an intermediate in the transfer pathway.

Relationship between Amplitude States and Primer Strand Pathway from the Polymerase Site to the Exonuclease Site—To address whether the upper amplitude state is one in which the primer strand has been transferred to the exonuclease active site, we used the N62D mutant of phi29 DNAP. This mutant enzyme is strongly compromised in its ability to stably transfer the primer strand of substrates bearing fully base-paired duplexes from the polymerase active site to the exonuclease active site (24). The impairment in stable primer strand binding at the exonuclease site caused by the N62D mutant shifts the equilibrium between the polymerase and exonuclease sites toward the polymerase site for DNA substrates with fully paired duplexes (24). We reasoned that if the upper amplitude state corresponded to an exonuclease complex, the impairment conferred by the N62D mutation would alter the equilibrium or the distance between the two amplitude states when complexes formed with the mutant enzyme were captured atop the nanopore.

The functional defect of the N62D mutant characterized for DNA substrates with 3′-OH-terminated primer strands (24) persisted when this enzyme was assayed with the substrate in Fig. 4*D*, *i*, which bears a 3′-H-terminated primer strand (Fig. 5*A*). Although the 3′-H-terminated substrate is a poorer exonuclease substrate than the equivalent DNA substrate bearing a 3′-OH terminus (19), the ddCMP terminus can be fully excised by the wild type enzyme (Fig. 5*A*, *lanes 1–8*). However, cleavage of this substrate by the N62D mutant was almost undetectable (Fig. 5*A*, *lanes 9–16*).

To determine whether the active site-proximal sequences that affect both the dwell time of complexes in the two states and the rate of exonucleolytic degradation with the wild type

FIGURE 4. **Active site-proximal DNA sequences influence the amplitude fluctuations of phi29 DNAP-DNA complexes atop the nanopore and the rate of 3′-5′-exonucleolytic cleavage in bulk phase.** *A*, sequences of the DNA1, DNA2, and DNA3 substrates. DNA2 differs from the DNA1 substrate (shown in full in Fig. 1*B*) in the T-A base pair (primer-template) at −2 of the duplex (highlighted in *purple*). DNA3 differs from the DNA1 substrate in the T-A base pair (primer-template) at −2 of the duplex (highlighted in *purple*) and from the DNA1 and DNA2 substrates in the dAMP residue at template position $n = 0$ (highlighted in *blue*). For DNA1, the −2 base pair is G-C and the $n = 0$ residue is dCMP. The three substrates are otherwise identical, including the abasic reporter from template positions +8 to +12 (shown as *red Xs*). Sixteen residues at the 5′-end of the template strand are not shown in this panel but can be seen in Fig. 1*B*. *B*, amplitude histograms (*blue curves*) for representative binary complexes formed with DNA1, DNA2, or DNA3 captured atop the nanopore at 180 mV. Histograms are fit to a two-term Gaussian function (*red curves*). Current trace segments from within the measured events are shown as *insets* in each histogram panel. *C*, quantity $p/(1 - p)$ (where p is the probability of the lower amplitude, post-translocation state) as a function of applied voltage for wild type phi29 DNAP-DNA binary complexes formed with DNA1 (*blue circles*), DNA2 (*red squares*), or DNA3 (*black triangles*). *D*, DNA substrates used in the exonuclease assays. Residues at the −2 base pair of the duplex (highlighted in *purple*) and at $n = 0$ of the template strand (highlighted in *blue*) in substrates *i*, *ii*, and *iii* correspond to those used in the nanopore assays, DNA1, DNA2, and DNA3, respectively; *5′-F*, 6-carboxy fluorescein. *E*, denaturing 22% polyacrylamide gels showing the products of phi29 DNAP-catalyzed exonucleolytic cleavage in nanopore buffer (20 mM K-Hepes, pH 8.0, 0.3 M KCl, 1 mM EDTA. and 1 mM DTT) for the three substrates shown in *D*. Mixtures containing 1 μM DNA substrate and 1.25 μM wild type phi29 DNAP were preincubated at 21 °C for 15 min prior to initiation of the exonuclease reaction by the addition of 10 mM $MgCl_2$. Reaction times at 21 °C are indicated. *F*, the fraction of full-length DNA substrate remaining as a function of time after the addition of 10 mM $MgCl_2$ for DNA i (*blue circles*), DNA ii (*red squares*), and DNA iii (*black triangles*).

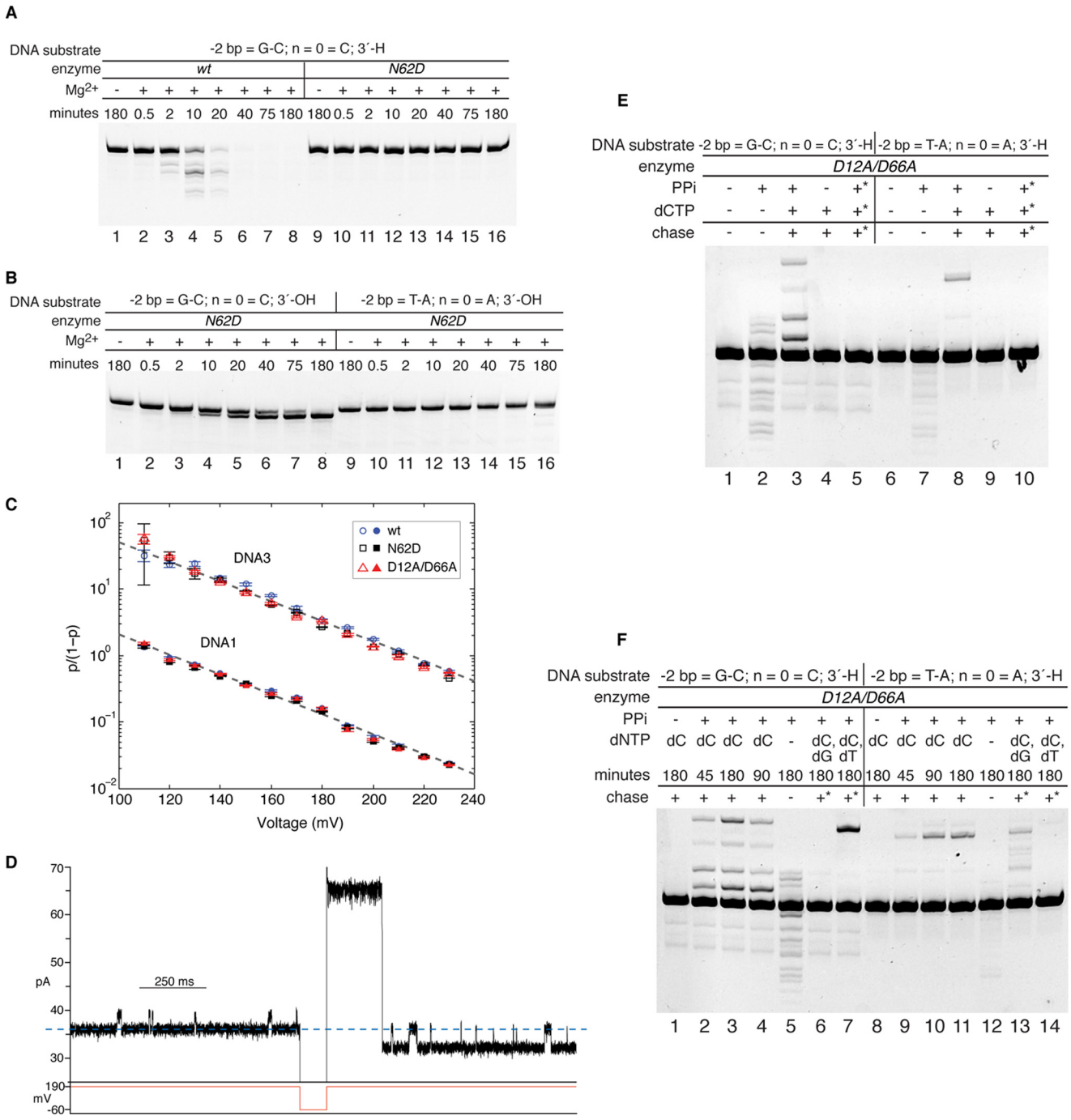

FIGURE 5. **Functional characteristics of phi29 DNAP complexes that correlate with the probability of upper amplitude occupancy.** *A*, denaturing 22% gel showing the products of exonuclease reactions catalyzed by wild type phi29 DNAP (*wt*, *lanes 1–8)* or N62D phi29 DNAP (*lanes 9–16*) in nanopore buffer using the DNA substrate with the sequence shown in Fig. 4*D*, *i*. *B*, denaturing gel showing the products of exonuclease reactions catalyzed by N62D phi29 DNAP in nanopore buffer using substrates with 3′-OH primer termini and the sequences shown in Fig. 4*D*, *i* (*lanes 1–8* here), and Fig. 4*D*, *iii* (*lanes 9–16* here). *C*, quantity $p/(1-p)$ (where p is the probability of the lower amplitude, post-translocation state) as a function of applied voltage for phi29 DNAP-DNA binary complexes formed with the DNA1 substrate (*filled symbols*) or the DNA3 substrate (*open symbols*) shown in Fig. 4*A*. Complexes were formed with wild type phi29 DNAP (*blue circles*), the N62D enzyme (*black squares*), or the D12A/D66A enzyme (*red triangles*). *Error bars* indicate the standard error. *D*, real-time current trace at 190 mV applied potential showing the latter part of a capture event for an N62D phi29 DNAP-DNA complex formed with the substrate shown in Fig. 2*D*, *iii*, followed directly by a capture of a complex with the substrate shown in Fig. 2*D*, *ii*. Both DNA substrates (0.5 μM each), N62D phi29 DNAP (1 μM), and 40 μM dGTP were present in the nanopore *cis* chamber. To maximize the number of complexes sampled during individual experiments, events that lasted longer than 30 s were terminated by a voltage reversal to −60 mV to eject the complex from atop the pore. *E* and *F*, denaturing gels showing the products of reactions catalyzed in nanopore buffer by D12A/D66A phi29 DNAP with the DNA substrates shown in Fig. 4*D*, i (*E*, *lanes 1–5*; *F*, *lanes 1–7*) or Fig. 4*D*, *iii* (*E*, *lanes 6–10*; *F*, *lanes 8–14*). Mixtures containing 1 μM DNA substrate, 1.25 μM D12A/D66A phi29 DNAP, and dNTPs and pyrophosphate (3 mM) as indicated were preincubated at 21 °C for 15 min prior to initiation of the reactions by the addition of 10 mM $MgCl_2$ and incubation at 30 °C for 180 min (*E*) or the times indicated (*F*). Where indicated, dCTP was present at 400 μM. The indicated reactions were followed by a chase step (composed of 250 μM each dATP, dGTP, and dTTP unless otherwise indicated below) conducted at 21 °C for 12 min. In *E*, *lanes 5* and *10* (denoted by *asterisks*), all reaction components including the chase mixture were incubated in the presence of $MgCl_2$ at 21 °C for 12 min (chase incubation conditions only). The reactions shown in *F*, *lanes 6* and *13*, included 400 μM dGTP in the 30 °C incubation, and the chase was composed of 250 μM each dATP and dTTP; in *F*, *lanes 7* and *14*, the 30 °C reactions included 400 μM dTTP, and the chase was composed of 250 μM each dATP and dGTP. These *lanes* are also indicated by *asterisks*.

enzyme also affected exonucleolytic cleavage catalyzed by the N62D enzyme, we used 3′-OH-terminated versions of the substrates shown in Fig. 4*D*, *i* and *iii*. Although slow cleavage of the substrate with the sequence that biases complexes toward the upper amplitude state by the N62D enzyme was observed (Fig. 5*B*, *lanes 1–8*), cleavage of the substrate that biases complexes toward the lower amplitude (post-translocation) state was barely detectable (Fig. 5*B*, *lanes 9–16*). Thus despite the impairment of the N62D in the productive transfer of a fully paired primer strand to the exonuclease site, this mutant enzyme exhibits the same sequence preference as the wild type enzyme.

When complexes formed with the N62D enzyme were examined in nanopore experiments, the fluctuations between amplitude states were virtually indistinguishable from complexes formed with the wild type enzyme (Fig. 5*C* and supplemental Fig. S5). The equilibrium between the two states was the same for binary complexes formed with the wild type and N62D enzymes; this was true for both the DNA1 and DNA3 sequence variants at voltages from 110 to 230 mV (Fig. 5*C*). The rates of transitions between the states appear nearly identical for binary complexes formed with both enzymes (supplemental Fig. S5). In addition, the distance of the template displacement observed for the N62D enzyme was indistinguishable from the distance observed for the wild type enzyme (Fig. 5, *C* and *D*, and Table 1). Therefore, the upper amplitude state is not one in which the primer strand has been transferred to the exonuclease active site. These data are consistent with the proposal that the upper amplitude state is an intermediate on the strand transfer pathway that is traversed prior to the step impaired by the N62D mutation.

What Is the Nature of the Proposed Intermediate on the Transfer Pathway?—The distance, direction, and effects of voltage on the template displacement that occurs in phi29 DNAP complexes are consistent with the hypothesis that when complexes are in the upper amplitude state, the primer-template junction is in the polymerase active site in the pre-translocation state. This model predicts that the DNA substrate with the sequence that biases complexes toward the upper amplitude state would serve as a superior substrate for pyrophosphorolysis. This reaction is the reverse of phosphodiester bond formation and is thus catalyzed in the pre-translocation state.

To compare the relative rates of the first pyrophosphorolytic cleavage for the two DNA substrates, we used the D12A/D66A mutant of phi29 DNAP, which lacks two of the aspartate residues essential for binding the catalytic divalent metal ions at the exonuclease active site and thus has negligible exonucleolytic activity (25, 26). As with the N62D enzyme, the amplitude fluctuations on the nanopore for complexes formed with the D12A/D66A enzyme and each of the two DNA substrate sequence variants were indistinguishable from complexes formed with the wild type enzyme (Fig. 5*C* and supplemental Fig. S5).

With the D12A/D66A enzyme, no extension of 3′-H-terminated substrates by the polymerase should occur in the presence of dNTPs unless the 3′-ddNMP residue is first excised by pyrophosphorolysis and exchanged for dNTP. Therefore, all DNA molecules bearing a 3′-OH terminus that accumulate in the presence of pyrophosphate should be directly dependent upon the first ddNTP excision. We conducted pyrophosphorolysis reactions using 3′-H-terminated DNA substrates in the presence of a high concentration of dCTP (400 μM) so that when the terminal ddCMP residue of a molecule was cleaved, if a residue was re-added by the polymerase there would be a high probability that it would be dCMP. We followed the initial reactions with a chase containing the remaining three dNTPs, the goal being to drive all products of initial ddCMP cleavage forward into extension products.

As expected with the D12A/D66A enzyme and 3′-H-terminated DNA substrates, no excision products were observed in the absence of pyrophosphate (Fig. 5*E*, *lanes 1* and *6*), and no excision or primer extension products were generated when dNTPs were added to reactions that had not been exposed to pyrophosphate (Fig. 5, *E*, *lanes 4* and *9*, and *F*, *lanes 1* and *8*). Although bands smaller than the full-length substrates are visible in the long gel exposures necessary for this experiment (particularly for the substrate in Fig. 5, *A*, *lanes 1–5*, and *B*, *lanes 1–7*), these bands are not due to a low level of exonuclease activity catalyzed by the D12A/D66A enzyme (supplemental Fig. S6) but are contaminants that persisted through two sequential gel purifications and are present without enzyme. Importantly, these bands were non-extendable with or without exposure to pyrophosphate (see below) and thus do not complicate the interpretation of the experiments.

In reactions conducted with pyrophosphate but without dNTPs, more pyrophosphorolysis products appeared to be generated with the DNA substrate with the sequence that biases complexes toward the upper amplitude state than with the substrate sequence that biases complexes toward the lower amplitude state (compare Fig. 5, *E*, *lane 2* with *7*, and *F*, *lane 5* with *12*). All of the detectable pyrophosphate-dependent products, but none of the minor contaminants, were driven into primer extension products by the chase (Fig. 5, *E*, *lanes 3* and *8*, and *F*, *lanes 2–4* and *9–11*). This allowed us to quantify the products of greater size than the starting DNA substrates, to approximate the extent of the first pyrophosphorolytic cleavage for the two DNA substrates. We determined the fraction contributed by the counts in the extended bands to the sum of the counts in the unextended band and the extended bands in the lane. For example, after 90 min at 30 °C in the presence of pyrophosphate and dCTP followed by the chase, these fractions were 0.261 (five independent experiments; S.E. 0.014) for the substrate with the sequence that biases complexes toward occupancy of the upper amplitude state and 0.139 (five independent experiments; S.E. 0.01) for the substrate with the sequence that biases complexes toward occupancy of the lower amplitude (post-translocation) state.

When the DNA substrates were incubated with pyrophosphate in the presence of all four dNTPs, no excision or extension products were detectable (Fig. 5*E*, *lanes 5* and *10*). This may be because of the simultaneous incubation with pyrophosphate and the dNTP complementary to $n = 0$ (dGTP or dTTP) for each of the substrates. Because pyrophosphorylysis occurs when complexes are in the pre-translocation state, it can be predicted that complementary dNTP would specifically inhibit the first pyrophosphorolytic cleavage for 3′-H-terminated

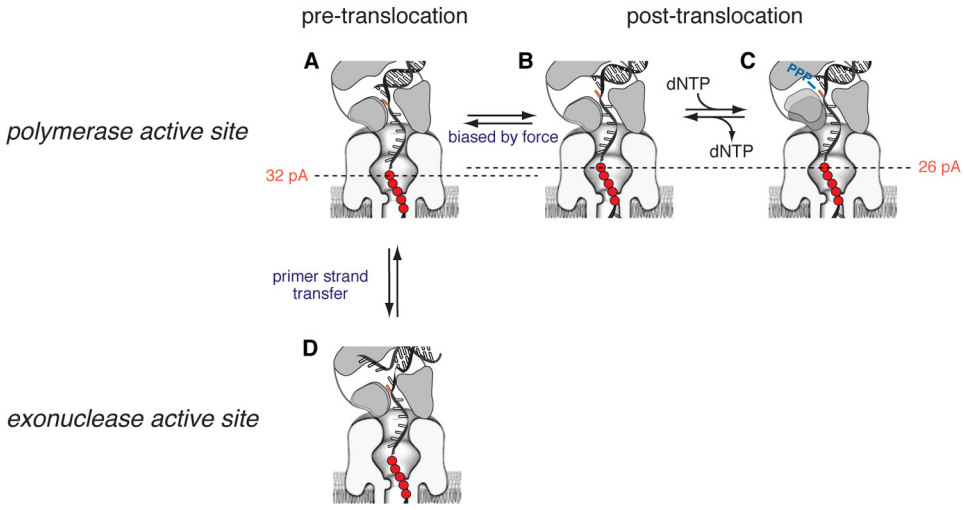

FIGURE 6. **Schematic illustration of a model for the states of phi29 DNAP-DNA complexes observed on the nanopore.** Immediately following phosphodiester bond formation, phi29 DNAP-DNA complexes are in the pre-translocation state (*A*) with the primer-template junction in the polymerase active site. Driven by Brownian thermal motion, the binary complexes oscillate between the pre-translocation (*A*) and post-translocation (*B*) states in the polymerase active site. The translocation equilibrium is influenced by active site-proximal DNA sequences and is biased toward the pre-translocation state by force on the template strand. Complexes can be rectified in the post-translocation state by the binding of complementary dNTP (*C*). When the primer strand of the DNA substrate bears a 3′-H terminus, complementary dNTP binds to and unbinds from the post-translocation complex. During processive synthesis, when the DNA substrate bears a 3′-OH terminus, complementary dNTP binding drives the complex forward through the nucleotide addition cycle. The pre-translocation state (*A*) is also a branch point from which the primer strand can be transferred to and from the exonuclease active site (*D*). In these schematics, the abasic residues spanning positions +8 to +12 of the template strand are shown as *red circles*, and the nucleotide at position $n = 0$ is highlighted is in *orange*. The fingers-closing transition that accompanies complementary dNTP binding is illustrated in *C*. The *horizontal dashed lines* indicate the displacement of the template strand in the nanopore lumen by a distance of ~1 nucleotide that reports the changes in register of the DNA substrate with respect to the enzyme during the transitions between the pre-translocation and post-translocation states.

DNA substrates by increasing the fraction of time spent in the post-translocation state. We tested this prediction directly by conducting incubations with pyrophosphate, dCTP, and either dGTP (Fig. 5*F*, *lanes 6* and *13*) or dTTP (Fig. 5*F*, *lanes 7* and *14*) followed by a chase with the remaining two dNTPs. For both DNA substrates, pyrophosphorolysis was specifically inhibited by the dNTP complementary to $n = 0$ (Fig. 5*F*, *lanes 6* and *14*). Taken together, the experiments in Fig. 5 indicate that the relative rates of pyrophosphorolysis for phi29 DNAP complexes with DNA substrates bearing the two sequences correlate with their relative probabilities to occupy the upper amplitude state atop the nanopore, consistent with a model in which the upper amplitude state is one in which the primer-template junction of the DNA substrate resides in the polymerase active site in the pre-translocation state.

DISCUSSION

Individual phi29 DNAP complexes formed with DNA substrates bearing fully base-paired duplexes fluctuate between two states on the millisecond time scale when captured in an electric field atop the α-HL nanopore. This fluctuation is due to a movement of the phi29 DNAP complex atop the pore that displaces the template strand with respect to the nanopore lumen by the distance of approximately a single nucleotide and that is detected as a change in ionic current amplitude reported by five consecutive abasic residues in the template strand (Fig. 6, *A* and *B*). One of the two amplitude states (the lower amplitude state with the abasic reporter used in this study, ~26 pA at 180 mV applied potential; Fig. 6*B*) can be assigned as one in which the primer-template junction of the DNA substrate resides in the polymerase active site in the post-translocation state, as this state can be stabilized by dNTP complementary to the templating base at $n = 0$ (Fig. 6*C*). When complexes move from the post-translocation state (Fig. 6*B*) to the upper amplitude state (~32 pA at 180 mV applied potential; Fig. 6*A*), the abasic reporter in the template strand moves further away from the enzyme complex atop the pore (further toward the *trans* chamber). Force applied on the template strand (voltage) biases complexes toward the upper amplitude state (Fig. 6, *A* and *B*). Based upon the distance and direction of the template movement and the effect of voltage on the equilibrium between the two states, we propose that the upper amplitude state is one in which phi29 DNAP-DNA complexes reside in the polymerase active site in the pre-translocation state (Fig. 6*A*).

Although the binding affinity for complementary dNTP when complexes are in the post-translocation state is high ($K_d \approx 1.4$ μM), it is negligible for complexes in the pre-translocation state, and the rate of transition from the pre-translocation state to the post-translocation state appears to be unaffected by dNTP (Fig. 3). These data support a model in which phi29 DNAP translocation occurs discretely from the pre-translocation state to the post-translocation state, driven by Brownian thermal motion. Binary complexes fluctuate between the pre-translocation and post-translocation states and are rectified to the post-translocation state by the binding of complementary dNTP.

A comparison of DNAP crystal structures for binary complexes in the fingers-open conformation and ternary complexes in the fingers-closed conformation has revealed active-site steric constraints that preclude pre-translocation state binding of the fully paired duplex product of correct nucleotide addition in the fingers-open state. Although the structural details differ, such constraints have been observed for both A and B family

DNA polymerases (4, 7). For phi29 DNAP binary complexes to move from the open, post-translocation state represented in the crystal structure (4) to the pre-translocation state (as occurs when complexes oscillate on the nanopore), there presumably must be a mechanism to avoid the steric clash of the primer terminus with residues Tyr-254 and Tyr-390, which occlude the nucleotide insertion site when the fingers are open. If phi29 DNAP binary complexes are in equilibrium between the fingers-open and fingers-closed states, as shown by smFRET for the A-family polymerase KF (27), this steric block may be relieved in a closed binary complex, permitting the movement to the pre-translocation state. Indeed, a candidate for such a closed binary complex, captured in the pre-translocation state, was observed in a recent structure of a chimeric RB69-UL54 B-family DNAP (28). The amplitude fluctuations observed in complexes atop the pore may thus reflect an equilibrium between the fingers-open and fingers-closed states inherent in phi29 DNAP-DNA binary complexes.

The equilibrium between the pre- and post-translocation states can be modulated by DNA sequences in the vicinity of the polymerase active site (Figs. 5*C* and 6*B*). Consistent with the proposal that the upper amplitude state corresponds to the pre-translocation state, a DNA substrate with a sequence that biases complexes toward occupancy of the upper amplitude state is a better substrate for pyrophosphorolysis than one with a sequence that biases complexes toward the lower amplitude state (Fig. 5). There is also a positive correlation between substrate sequence bias toward the upper amplitude state for complexes on the pore and a faster rate of exonuclease activity in bulk phase (Fig. 4), which implicates the upper amplitude state in the pathway for transfer of the primer strand from the polymerase to exonuclease active site. However, the oscillations measured for complexes formed with the N62D mutant enzyme do not differ significantly from those measured for complexes formed with the wild type enzyme (Fig. 5). Therefore we propose that the pre-translocation state is a branch point that occurs prior to the step at which the N62D mutation exerts its effect. From this state, the DNA substrate in phi29 DNAP complexes can proceed either to the post-translocation state (Fig. 6, *A* and *B*) or to the exonuclease active site (Fig. 6, *A* and *D*). A pathway in which the pre-translocation state is a branch point in primer strand transfer between the polymerase and exonuclease active sites is also suggested from crystal structures of RB69 DNAP binary complexes formed with a DNA substrate bearing a furan-dAMP mismatch at the duplex terminus (29). For complexes in two of the copies of the crystal asymmetric unit, the DNA substrate occupied the polymerase active site in the fingers-open, pre-translocation state, whereas for the complex in one copy, the primer strand was melted into the exonuclease active site. Such a pathway implies that during DNA synthesis the commitment to send the primer terminus to the exonuclease site after nucleotide incorporation precedes translocation.

In this study, we have observed directly the translocation step of the phi29 DNAP catalytic cycle at the single molecule level and have quantified the equilibrium across this step as a function of applied force, active site-proximal DNA sequences, and incoming dNTP concentration. This leaves us poised to address the mechanisms by which these factors, as well as duplex mismatches, affect the fate of complexes at this branch point. In a study concurrent with this one (to be presented elsewhere), we have quantified the forward and reverse rates of the transitions between the pre-translocation and post-translocation states, as well as the rates of dNTP binding and dissociation in the post-translocation state. This will permit the mechanisms governing the pathway to be addressed in a kinetic framework. Because phi29 DNAP-catalyzed DNA synthesis and exonucleolysis can be monitored with single nucleotide precision when complexes reside atop the nanopore (19), we can examine these mechanisms during processive reactions as well as under the equilibrium conditions employed in this current study.

Acknowledgments—We are grateful to colleagues at XPol Biotech who provided high quality mutant phi29 DNAP proteins in concentrated, detergent-free form. We thank Heidi Gomez (University of California, Santa Cruz) for indispensable help in acquiring reagents. We thank Jaryn Perkins and Jason Maydan at Boreal Genomics (Vancouver, British Columbia, Canada) for the use of gel imaging facilities and Peter Walker and Yen Tran at Stanford Protein and Nucleic Acid Facility for expert oligonucleotide synthesis. We are grateful to William Dunbar for helpful discussions.

REFERENCES

1. Hariharan, C., Bloom, L. B., Helquist, S. A., Kool, E. T., and Reha-Krantz, L. J. (2006) Dynamics of nucleotide incorporation: snapshots revealed by 2-aminopurine fluorescence studies. *Biochemistry* **45,** 2836–2844
2. Joyce, C. M., Potapova, O., Delucia, A. M., Huang, X., Basu, V. P., and Grindley, N. D. (2008) Fingers-closing and other rapid conformational changes in DNA polymerase I (Klenow fragment) and their role in nucleotide selectivity. *Biochemistry* **47,** 6103–6116
3. Zhang, H., Cao, W., Zakharova, E., Konigsberg, W., and De La Cruz, E. M. (2007) Fluorescence of 2-aminopurine reveals rapid conformational changes in the RB69 DNA polymerase-primer/template complexes upon binding and incorporation of matched deoxynucleoside triphosphates. *Nucleic Acids Res.* **35,** 6052–6062
4. Berman, A. J., Kamtekar, S., Goodman, J. L., Lázaro, J. M., de Vega, M., Blanco, L., Salas, M., and Steitz, T. A. (2007) Structures of phi29 DNA polymerase complexed with substrate: the mechanism of translocation in B-family polymerases. *EMBO J.* **26,** 3494–3505
5. Doublié, S., Tabor, S., Long, A. M., Richardson, C. C., and Ellenberger, T. (1998) Crystal structure of a bacteriophage T7 DNA replication complex at 2.2 A resolution. *Nature* **391,** 251–258
6. Franklin, M. C., Wang, J., and Steitz, T. A. (2001) Structure of the replicating complex of a pol α family DNA polymerase. *Cell* **105,** 657–667
7. Johnson, S. J., Taylor, J. S., and Beese, L. S. (2003) Processive DNA synthesis observed in a polymerase crystal suggests a mechanism for the prevention of frameshift mutations. *Proc. Natl. Acad. Sci. U.S.A.* **100,** 3895–3900
8. Beese, L. S., Friedman, J. M., and Steitz, T. A. (1993) Crystal structures of the Klenow fragment of DNA polymerase I complexed with deoxynucleoside triphosphate and pyrophosphate. *Biochemistry* **32,** 14095–14101
9. Eom, S. H., Wang, J., and Steitz, T. A. (1996) Structure of *Taq* polymerase with DNA at the polymerase active site. *Nature* **382,** 278–281
10. Kamtekar, S., Berman, A. J., Wang, J., Lázaro, J. M., de Vega, M., Blanco, L., Salas, M., and Steitz, T. A. (2004) Insights into strand displacement and processivity from the crystal structure of the protein-primed DNA polymerase of bacteriophage phi29. *Mol. Cell* **16,** 609–618
11. Wang, J., Sattar, A. K., Wang, C. C., Karam, J. D., Konigsberg, W. H., and Steitz, T. A. (1997) Crystal structure of a pol α family replication DNA polymerase from bacteriophage RB69. *Cell* **89,** 1087–1099
12. de Vega, M., Blanco, L., and Salas, M. (1999) Processive proofreading and the spatial relationship between polymerase and exonuclease active sites

of bacteriophage phi29 DNA polymerase. *J. Mol. Biol.* **292,** 39–51
13. Joyce, C. M. (1989) How DNA travels between the separate polymerase and 3′-5′-exonuclease sites of DNA polymerase I (Klenow fragment). *J. Biol. Chem.* **264,** 10858–10866
14. Baker, R. P., and Reha-Krantz, L. J. (1998) Identification of a transient excision intermediate at the crossroads between DNA polymerase extension and proofreading pathways. *Proc. Natl. Acad. Sci. U.S.A.* **95,** 3507–3512
15. Hariharan, C., and Reha-Krantz, L. J. (2005) Using 2-aminopurine fluorescence to detect bacteriophage T4 DNA polymerase-DNA complexes that are important for primer extension and proofreading reactions. *Biochemistry* **44,** 15674–15684
16. Ibarra, B., Chemla, Y. R., Plyasunov, S., Smith, S. B., Lázaro, J. M., Salas, M., and Bustamante, C. (2009) Proofreading dynamics of a processive DNA polymerase. *EMBO J.* **28,** 2794–2802
17. Blanco, L., and Salas, M. (1996) Relating structure to function in phi29 DNA polymerase. *J. Biol. Chem.* **271,** 8509–8512
18. Salas, M., Blanco, L., Lázaro, J. M., and de Vega, M. (2008) The bacteriophage phi29 DNA polymerase. *IUBMB Life* **60,** 82–85
19. Lieberman, K. R., Cherf, G. M., Doody, M. J., Olasagasti, F., Kolodji, Y., and Akeson, M. (2010) Processive replication of single DNA molecules in a nanopore catalyzed by phi29 DNA polymerase. *J. Am. Chem. Soc.* **132,** 17961–17972
20. Benner, S., Chen, R. J., Wilson, N. A., Abu-Shumays, R., Hurt, N., Lieberman, K. R., Deamer, D. W., Dunbar, W. B., and Akeson, M. (2007) Sequence-specific detection of individual DNA polymerase complexes in real time using a nanopore. *Nat. Nanotechnol.* **2,** 718–724
21. Cockroft, S. L., Chu, J., Amorin, M., and Ghadiri, M. R. (2008) A single-molecule nanopore device detects DNA polymerase activity with single-nucleotide resolution. *J. Am. Chem. Soc.* **130,** 818–820
22. Olasagasti, F., Lieberman, K. R., Benner, S., Cherf, G. M., Dahl, J. M., Deamer, D. W., and Akeson, M. (2010) Replication of individual DNA molecules under electronic control using a protein nanopore. *Nat. Nanotechnol.* **5,** 798–806
23. Garalde, D. R., Simon, C. A., Dahl, J. M., Wang, H., Akeson, M., and Lieberman, K. R. (2011) Distinct complexes of DNA polymerase I (Klenow fragment) for base and sugar discrimination during nucleotide substrate selection. *J. Biol. Chem.* **286,** 14480–14492
24. de Vega, M., Lazaro, J. M., Salas, M., and Blanco, L. (1996) Primer-terminus stabilization at the 3′-5′ exonuclease active site of phi29 DNA polymerase. Involvement of two amino acid residues highly conserved in proofreading DNA polymerases. *EMBO J.* **15,** 1182–1192
25. Bernad, A., Blanco, L., Lázaro, J. M., Martín, G., and Salas, M. (1989) A conserved 3′-5′ exonuclease active site in prokaryotic and eukaryotic DNA polymerases. *Cell* **59,** 219–228
26. Garmendia, C., Bernad, A., Esteban, J. A., Blanco, L., and Salas, M. (1992) The bacteriophage phi29 DNA polymerase, a proofreading enzyme. *J. Biol. Chem.* **267,** 2594–2599
27. Santoso, Y., Joyce, C. M., Potapova, O., Le Reste, L., Hohlbein, J., Torella, J. P., Grindley, N. D., and Kapanidis, A. N. (2010) Conformational transitions in DNA polymerase I revealed by single-molecule FRET. *Proc. Natl. Acad. Sci. U.S.A.* **107,** 715–720
28. Zahn, K. E., Tchesnokov, E. P., Götte, M., and Doublié, S. (2011) Phosphonoformic acid inhibits viral replication by trapping the closed form of the DNA polymerase. *J. Biol. Chem.* **286,** 25246–25255
29. Hogg, M., Wallace, S. S., and Doublié, S. (2004) Crystallographic snapshots of a replicative DNA polymerase encountering an abasic site. *EMBO J.* **23,** 1483–1493
30. Hurt, N., Wang, H., Akeson, M., and Lieberman, K. R. (2009) Specific nucleotide binding and rebinding to individual DNA polymerase complexes captured on a nanopore. *J. Am. Chem. Soc.* **131,** 3772–3778